JMEPEG (2009) 18:603–611
DOI: 10.1007/s11665-009-9358-1

1059-9495/$19.00

Factors Controlling Superelastic Damping Capacity of SMAs

L. Heller, P. Šittner, J. Pilch, and M. Landa

(Submitted October 26, 2008; in revised form December 2, 2008)

In this paper, questions linked to the practical use of superelastic damping exploiting stress-induced martensitic transformation for vibration damping are addressed. Four parameters, particularly vibration amplitude, prestrain, temperature of surroundings, and frequency, are identified as having the most pronounced influence on the superelastic damping. Their influence on superelastic damping of a commercially available superelastic NiTi wire was experimentally investigated using a self-developed dedicated vibrational equipment. Experimental results show how the vibration amplitude, frequency, prestrain, and temperature affect the capacity of a superelastic NiTi wire to dissipate energy of vibrations through the superelastic damping. A special attention is paid to the frequency dependence (i.e., rate dependence) of the superelastic damping. It is shown that this is nearly negligible in case the wire is in the thermal chamber controlling actively the environmental temperature. In case of wire exposed to free environmental temperature in actual damping applications, however, the superelastic damping capacity significantly decreases with increasing frequency. This was explained to be a combined effect of the heat effects affecting the mean wire temperature and material properties with the help of simulations using the heat equation coupled phenomenological SMA model.

Keywords shape memory alloys, superelastic damping, thermomechanical testing

1. Introduction

Taking advantage of the relatively large hysteresis, strain and stress amplitude as well as recentering capability, the superelastic deformation of shape memory alloys (SMAs) has been widely promoted as a phenomenon to be used for passive damping purposes (Ref 1-3). This superelastic damping capacity (SDC) of SMAs is commonly quantified based on the enclosed area of the superelastic stress-strain loop measured in quasistatic tensile test at room temperature. However, the relevance of such a quantification is questionable with regard to dynamic conditions the damping applications are subjected to. Many publications in the literature dealing with the high damping capacity of SMA are based on DMA studies of the internal friction damping performed at extremely low vibration amplitudes (Ref 4, 5). In reality, as everyone knows, the stresses and strains involved in SMA damping can be rather large and the dissipation energy through the stress-induced martensitic transformation (MT) may in fact reach even much higher values compared to the internal friction damping. In spite of the great potential of the superelastic damping, there seems to be only a limited knowledge of dynamic superelastic deformations of SMA wires subjected to dynamical excitations with higher strain amplitudes and frequencies. Most of existing literature deals with the superelastic hysteresis at rather low range of strain rates (Ref 6, 7). Although the literature focused on the engineering and applied mechanics provides studies of SMAs damping capacity in a wider range of amplitudes and frequencies (Ref 8), the quasistatic superelastic responses are still typically considered in modelling as well as in the design of passive damping applications based on SMA elements.

The present paper is aimed at analyzing the SDC of SMAs with particular respect to working conditions the SMA damper is subjected to in real applications. We consider a superelastic wire as the simplest representation of the SMA damper. For such a damper, we define four working conditions (see Fig. 1) that are supposed to have an important impact on the SDC. The first parameter represents the vibration amplitude that is basically given by the external load and geometry of the SMA damper. SMA dampers are installed with a predefined prestrain which is the second working condition. As the SMA behavior is strongly temperature dependent, the temperature of the wire surroundings is the third important parameter to be considered. The frequency of the external load to which the SMA damper is exposed represents the fourth condition one has to consider when designing a SMA damper. The influence of those four parameters on the SDC was analyzed by an experimental study carried out on a commercially available superelastic thin NiTi wire. The role of frequency (i.e. strain rate) is analyzed more deeply in the last part of this paper using a phenomenological SMA model coupled with a lumped-capacity heat equation. The rate dependence of the

This article is an invited paper selected from presentations at Shape Memory and Superelastic Technologies 2008, held September 21-25, 2008, in Stressa, Italy, and has been expanded from the original presentation.

L. Heller, P. Šittner, and **J. Pilch**, Institute of Physics, Academy of Sciences of the Czech Republic, Prague 18221, Czech Republic; and **M. Landa**, Institute of Thermomechanics, Academy of Sciences of the Czech Republic, Prague 18000, Czech Republic. Contact e-mail: heller@fzu.cz.

superelastic damping is finally rationalized and explained through simulations made with this model. It comes out of this analysis that the heat transfer through the wire surface (i.e. the ability of the environment to take the heat out of the wire) represents a fifth important condition which, however, was not particularly considered in present experimental investigations.

The working conditions introduced above represent a set of parameters within which one shall map the SDC of a given SMA damper in order to find optimal working conditions maximizing its damping efficiency as well as boundaries in the parameter space where the SDC becomes negligible. Results of such a mapping will help the potential designer of SMA damper who needs to take into account further requirements on the parameters additional to the maximal SDC of the SMA damper.

2. Experimental Identification of the Superelastic Damping

In order to realize experimentally the mapping of the SDC in the space of the four working conditions (vibration amplitude, frequency, prestrain, and temperature), a dedicated experimental equipment called AVUT (Fig. 2) was designed and built in the frame of AVALON project (Ref 8) focused on development of hybrid NiTi textiles with integrated thin NiTi wires. The equipment consists of an electromagnetic shaker mounted on a movable base that allows to prestrain the wire fixed between the shaker and the frame. The excitation provided by the shaker is measured by a piezoelectric accelerometer at the moving end of the studied wire where a load cell is also mounted ensuring the measurement of the mean force in the wire. The alternating

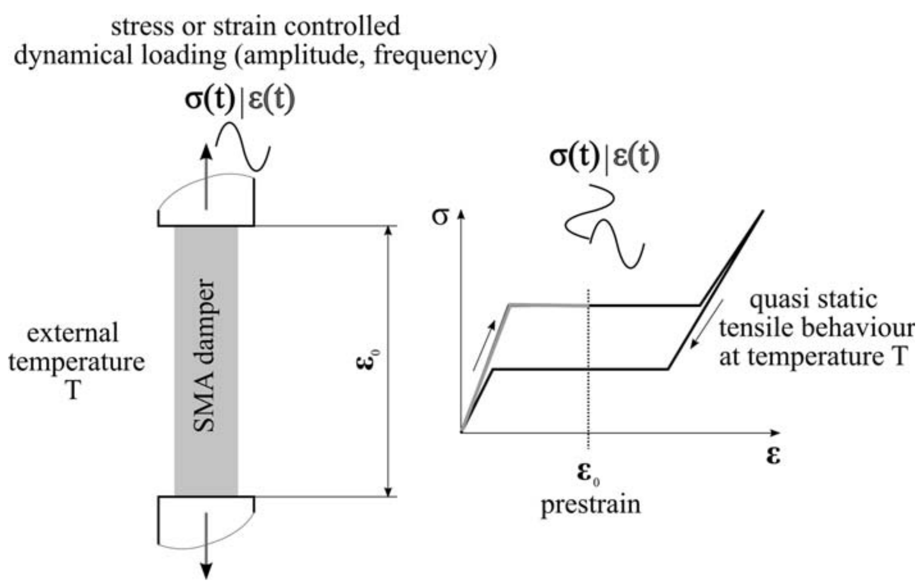

Fig. 1 Schematic representation of a simple 1D SMA damper and four working conditions to be considered in its design represented by the vibration amplitude, frequency, prestrain, and temperature

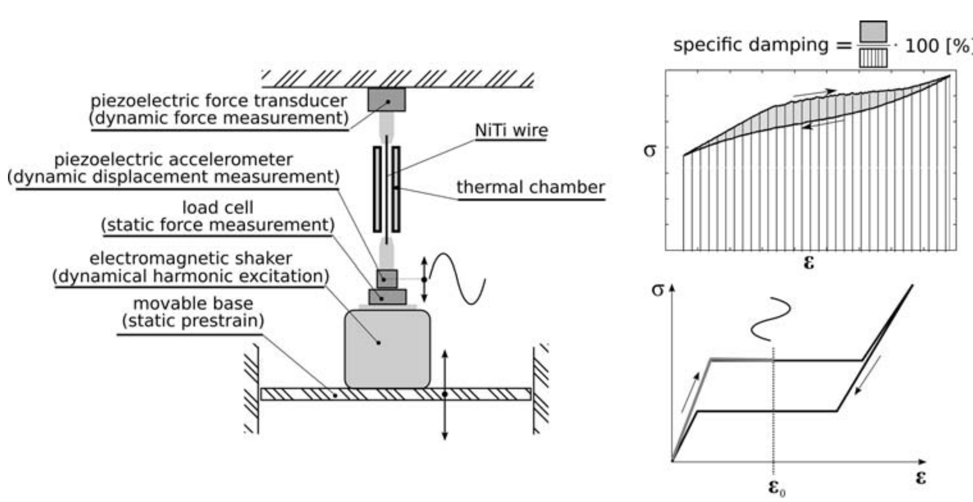

Fig. 2 Scheme with main components of the testing device for identification of the SDC and its dependence on working conditions. The upper right corner shows the definition of specific damping used for evaluating the damping capacity of the SMA wire

component of the force in the wire is measured through a piezoelectric force transducer attached to the fixed end of the wire. The temperature of the wire surroundings is controlled by a thermal chamber based on the Peltier elements. The system allows to measure the dynamic response of the SMA wire to a harmonic excitation with controlled strain amplitude, prestrain, frequency, and temperature. Three signals are simultaneously recorded in the experiments—the mean and alternating components of the force in the wire and the acceleration of the excited end of the wire. The experimental results in terms of stress-strain loop, its area, and corresponding specific damping (see Fig. 2 for its definition) are extracted from measured data.

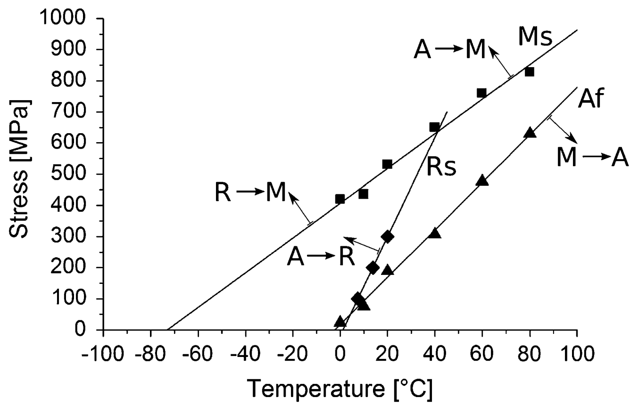

Fig. 3 Non-equilibrium stress-temperature diagram of the tested superelastic NiTi wire where the transformation lines represent the temperature dependence of transformation stresses for austenite to martensite, martensite to austenite, and austenite to R-phase transformation

3. Effect of Working Conditions on the Superelastic Damping

The AVUT equipment was used to investigate the effect of the working conditions on the SDC of a commercially available superelastic NiTi wire (55 wt.% Ni) of diameter 100 μm. The wire supplied in already heat-treated conditions was first analyzed and characterized under quasistatic loadings using the approach described in detail in Ref 9. This approach led to a quantification of thermomechanical properties of the wire via evaluation of 23 material parameters (selected ones are listed in Table 1) and construction of the non-equilibrium stress-temperature diagram (Fig. 3). As a specific property of this particular wire, one can notice that the superelastic hysteresis decreases with increasing temperature (as evidenced by the converging M_s and A_f transformation lines in the stress-temperature diagram).

The dynamical testing of the superelastic NiTi wire was performed in such a way that a virgin sample of gauge length 50 mm was excited at given working conditions until its failure. A characteristic wire response in terms of evolution of displacement and specific damping in case of test in which the strain amplitude, frequency, and environment temperature was prescribed is shown in Fig. 4. One can see that the wire response is dramatically changing in the first 2 s (~100 cycles) in a region denoted "unsteady vibrations". Later on in the stable vibration region, however, the SDC evolves as well although in much lesser extent. There are basically two factors contributing to the evolution of damping response with the number of cycles. These are the heat generated/absorbed by the vibrating wire and microstructural changes in the wire leading to variation of its stress-strain response.

The specific damping capacity (see Fig. 2 for its definition) decreases in the unsteady vibration stage down to a characteristic value (~12% in Fig. 4) as the wire vibrations settle into

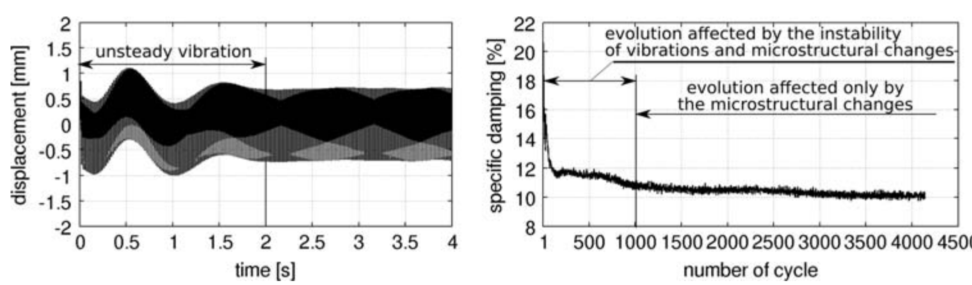

Fig. 4 Vibration test in which the strain amplitude (2%), frequency (50 Hz), and environment temperature (295 K) was prescribed. On the left-hand side, a typical time response in terms of displacement of the excited wire tip is shown with depicted unsteady stage of vibrations; on the right-hand side, a characteristic evolution of specific damping with number of cycles is given

Table 1 Selected material parameters of the tested wire obtained from quasistatic thermomechanical testing

NiTi 100 μm													
M'_s, °C	A'_f, °C	R_s, °C	$S_{A\text{-}M}$, MPa/°C	$S_{A\text{-}R}$, MPa/°C	$S_{M\text{-}A}$, MPa/°C	σ_{UTS}, MPa	σ_Y, MPa	σ_{tr}, MPa	Δh_σ, MPa	ε_{tr}, %	ε_f, %	E_m, GPa	E_a, GPa
−72	0	−11	5.7	16.5	7.5	1600	1330	550	340	5.2	13	21	54

M'_s/A'_f effective martensite/austenite start/finish temperature; R_s R-phase start temperature; $S_{A\text{-}M}/S_{A\text{-}M}/S_{A\text{-}R}$ temperature dependences of transformation stress for A-M/M-A/A-R; σ_{UTS} ultimate tensile strength; σ_Y yield stress; σ_{tr} transformation yield stress of austenite at RT; Δh_σ superelastic stress hysteresis at RT; ε_{tr} maximum recoverable transformation strain; ε_f strain at failure; E_a/E_m Young modulus of austenite/martensite the steady state meaningful for the damping applications. Since this is observed on the virgin wire as well as on the already cycled wires, we believe this unsteady region is mainly due to the heat effects as will be discussed below. The cyclic tensile loading is, however, also accompanied by microstructural changes taking place in the SMA wire which are known to be most pronounced at the early stage of cycling. Both effects thus affect the SDC particularly in the unsteady vibration range and can be hardly distinguished. The effect of microstructural changes on the damping capacity of the SMA wire can, however, be very well identified in the steady vibrations range (see Fig. 4), where the heat effects are completely stable. In order to evaluate the effect of the four parameters on the SDC of the studied NiTi wire, the specific damping and energy dissipation within one period of motion in the steady vibration range at the 1000th cycle were taken as characteristic values.

In this paper, we basically attempt to demonstrate the importance of the effect of the used working conditions when applying the superelastic damping as a damping mechanism in passive damping elements. Hence, the SDC of the studied wire was mapped in the space of the four parameters using a simplified approach supposing that a change in one working parameter does not affect the influence of other parameters on the SDC. This is not correct for many combinations of parameters. However, we have tried to select parameters in the ranges where this is approximately true. Therefore, the influence of one working parameter was studied by varying its value around a basic level and measuring the corresponding SDC while keeping the remaining working parameters constant. The basic level of all four parameters was chosen as follows: prestrain 4% in the middle of the plateau, amplitude 1.2%, temperature 20 °C, frequency 50 Hz.

3.1 The Influence of Prestrain

SMA elements used in dampers are usually installed with a defined prestrain for two main reasons. In case of tension, the prestrains avoid the compressional load that would lead to buckling and damage. In addition, when a superelastic SMA element is prestrained to a partially transformed state, the strain amplitude necessary to initiate the superelastic damping mechanism and hence significant damping is much lower than in the case of an unprestrained SMA element. However, the level of prestraining affects presumably the SDC. This expected effect was studied by measuring the SDC at four different levels of prestrain distributed along the plateau as schematically shown in Fig. 5. Corresponding stress-strain loops measured at 1000th cycle are displayed in Fig. 6.

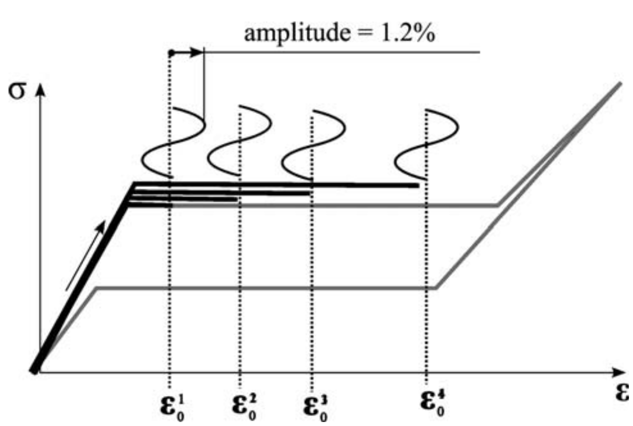

Fig. 5 Schematic representation of four prestrains at which the SDC was evaluated

As one can notice in Fig. 6, the stress-strain loop area decreases with increasing prestrain that is more evident when plotting directly the loop areas (Fig. 7) and specific damping versus prestrain (Fig. 8). The dissipated energy per cycle is very low in the elastic range, increases with increasing prestrain reaching a local maximum at the first third of the plateau range, and decreases as much as 60% toward the end of the plateau. The specific damping capacity shows basically a similar trend.

3.2 The Influence of Vibration Amplitude

A vibrating prestrained SMA element always deforms partially elastically and partially due to stress-induced MT

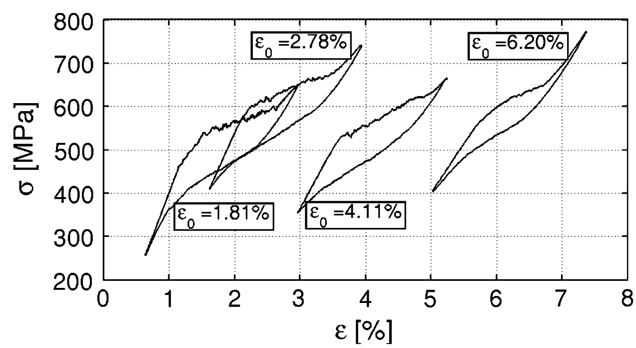

Fig. 6 Stress-strain loops measured at four prestrains while keeping the other working conditions at the basic level, i.e. amplitude 1.2%, temperature 20 °C, and frequency 50 Hz

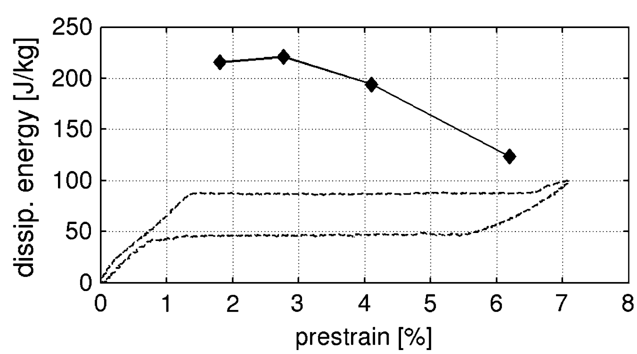

Fig. 7 Plot of dissipated energy vs. prestrain

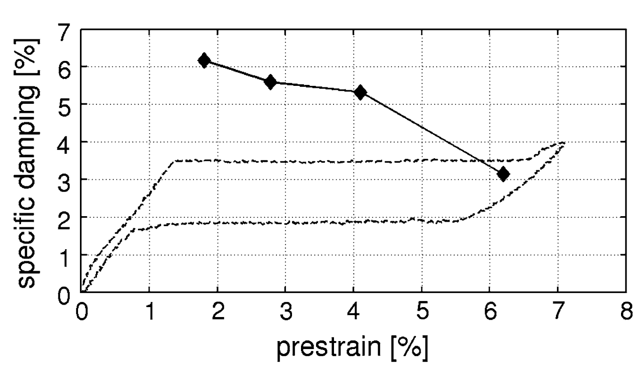

Fig. 8 Plot of specific damping vs. prestrain

responsible for damping. With increasing vibration amplitude, the fraction of the latter and consequently the damping capacity increases. However, in the lower end, the mechanical excitation has to be sufficiently large in order to give rise to deformation beyond this elastic range. In other words, if the superelasticity is being used for damping purposes, the amplitude of vibrations has to be at least slightly higher than the elastic deformation the prestrained SMA element is capable of at the given prestrain, frequency, and temperature. Although this is generally known, it is violated in many SMA damping applications, since the designers tend to decide for lower amplitudes due to the fatigue constraints.

At any circumstances, knowledge of the evolution of the SDC with increasing vibration amplitude is important for the efficient use of SMAs in damping applications. We evaluated the effect of increasing strain amplitude on the SDC for five different strain amplitudes as illustrated in Fig. 9 and 10. The transition from almost purely elastic deformation to the superelastic one when increasing vibration amplitude is clearly seen on the evolution of stress-strain loops shown in Fig. 10. Such a transition is reflected by an exponential increase of the dissipated energy with increasing strain amplitude (see Fig. 11) which saturates beyond the 3% level. The corresponding specific damping evolution increases as seen in Fig. 12 and reaches maximum at 3%. Minimum strain amplitude of 0.5% is needed for obtaining a reasonably high superelastic damping from the present wire at the given prestrain, frequency, and temperature.

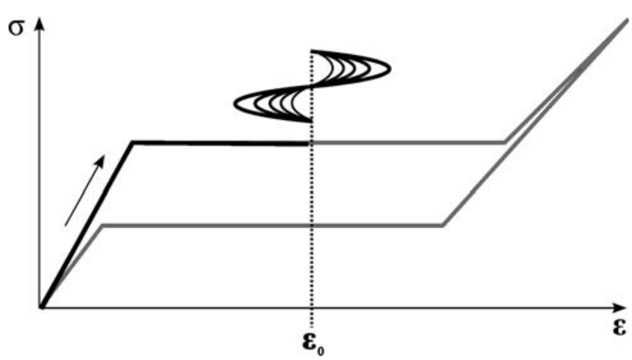

Fig. 9 Schematic representation of five amplitudes at which the SDC was evaluated

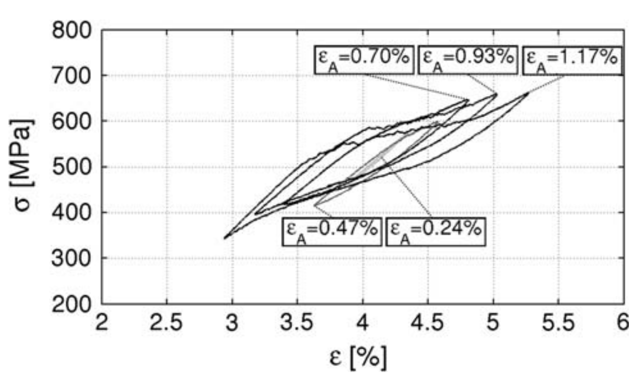

Fig. 10 Stress-strain loops measured at five amplitudes while keeping the other working conditions at the basic level, i.e. prestrain 4%, temperature 20 °C, and frequency 50 Hz

4. The Influence of Temperature

The temperature dependence of SMA behavior is generally assumed in term of Clausius-Clapeyron relation that is, however, directly applicable only to a single crystal specimen. According to this relation, no temperature dependence of the superelastic hysteresis shall be expected. However, when dealing with polycrystalline material, the Clausius-Clapeyron relation represents a certain approximation. As it was mentioned above, the stress-temperature diagram of the studied wire shows the M_s and A_f transformation lines that are not parallel as predicted by Clausius-Clapeyron relation but converge one to the other, i.e. the stress hysteresis decreases with increasing temperature. Hence, the temperature can be considered in some cases as a relevant working condition influencing the SDC. In the present work, the sensitivity of the SDC to temperature changes was analyzed in a range between 10 and 65 °C. At each temperature, the wire was prestrained to the middle of the plateau, i.e. the prestrain was not constant but linearly increasing with increasing temperature to compensate the increase of the plateau stress as illustrated in Fig. 13. The stress-strain loops for different temperatures obtained under dynamic loading (see Fig. 14) reveal clearly the tendency to decrease the hysteresis with increasing temperature as in the case of quasistatic tensile loading (see stress-temperature diagram in Fig. 3).

The dramatic effect of the temperature on the SDC is evidenced by temperature evolutions of the dissipated energy and specific damping shown in Fig. 15 and 16. One can notice that the temperature change from 10 to 65 °C is accompanied by a decrease of the dissipated energy per cycle and specific

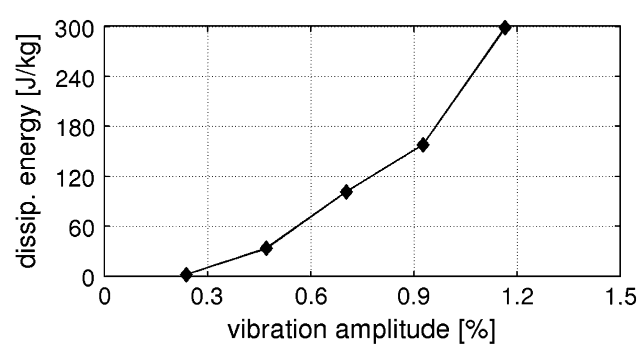

Fig. 11 Plot of dissipated energy vs.vibration amplitude

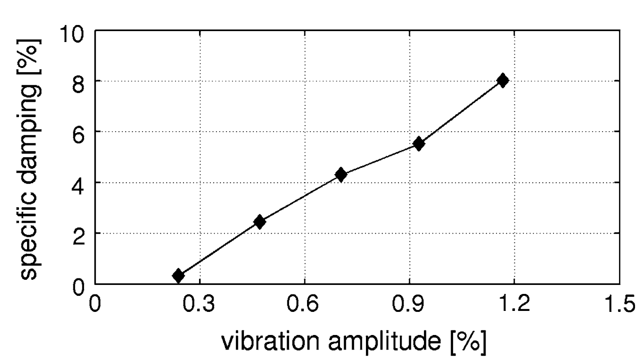

Fig. 12 Plot of specific damping as a function of the vibration amplitude

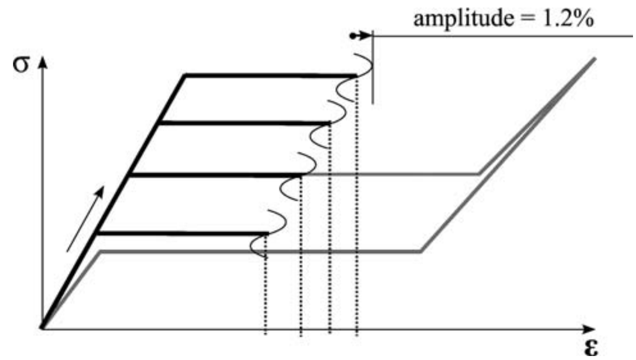

Fig. 13 Schematic representation of stress-strain curves corresponding to prestrains at four temperatures at which the SDC was evaluated

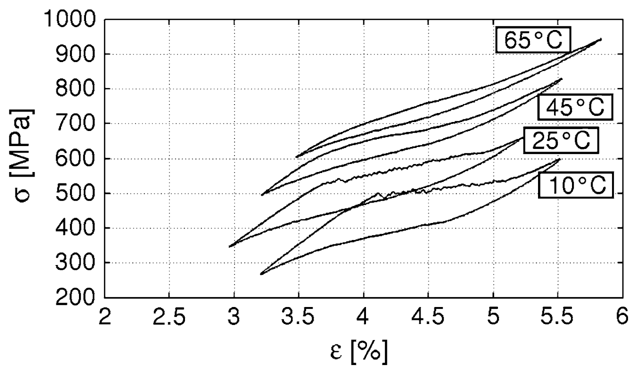

Fig. 14 Stress-strain loops measured at four temperatures while keeping the other working conditions at the basic level, i.e. prestrain 4%, amplitude 1.2%, and frequency 50 Hz

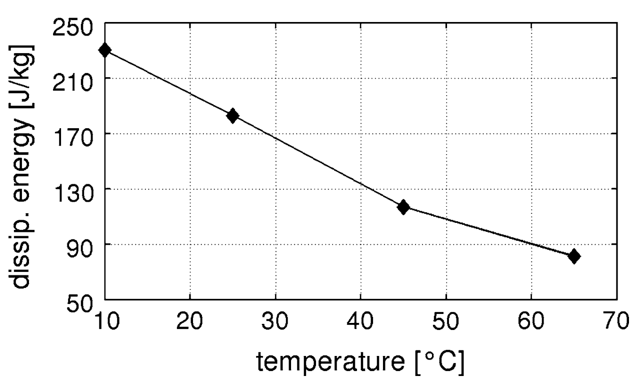

Fig. 15 Plot of dissipated energy vs. temperature of surroundings

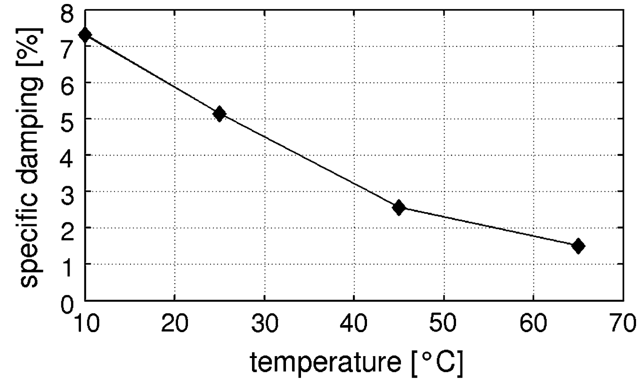

Fig. 16 Plot of specific damping as a function of temperature of surroundings

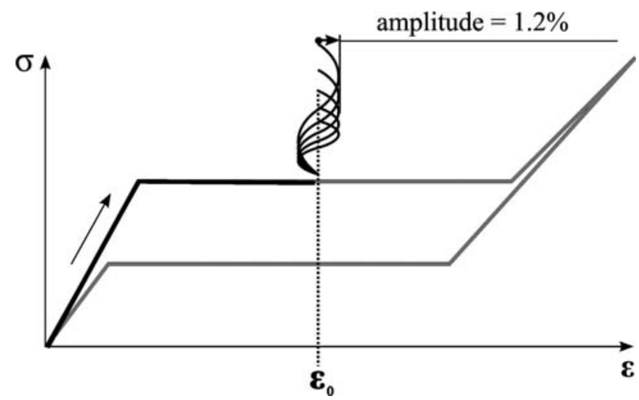

Fig. 17 Schematic representation of five frequencies at which the SDC was evaluated

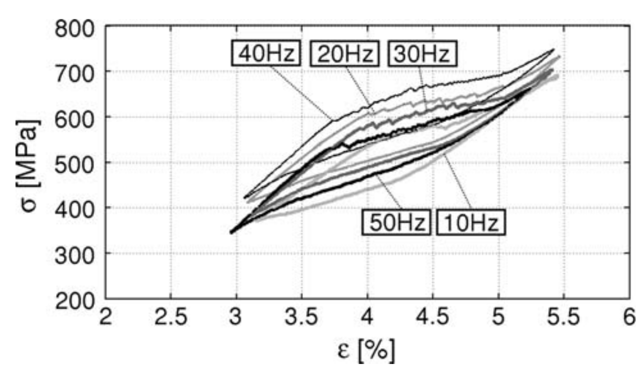

Fig. 18 Stress-strain loops (1000th) measured at five frequencies while keeping the other working conditions at the basic level, i.e. prestrain 4%, amplitude 1.2%, and temperature 20 °C

damping as large as 65 and 85%, respectively. However, since the heat and microstructural effects may also be involved in this decrease, we do not expect it to be solely due to the above discussed decrease of the stress hysteresis with increasing temperature.

5. The Influence of Frequency

SMA dampers are commonly considered for damping low frequency vibrations. Can we use it for higher frequencies as well? How the frequency affects the SDC and where is the high frequency limit? The frequency is yet another working condition with respect to which the SDC of SMA elements should be evaluated. We investigated the SDC of the present wire in the frequency range 10-50 Hz (Fig. 17). The results are shown in Fig. 18-20. The stress-strain loops do not display substantial differences in this frequency range as can be seen in Fig. 18. Neither the stress-strain loop areas nor the damping capacity seems to be significantly affected by the frequency change in this frequency range.

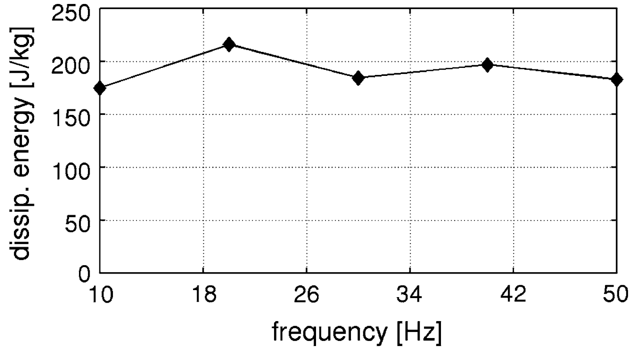

Fig. 19 Plot of dissipated energy vs. frequency

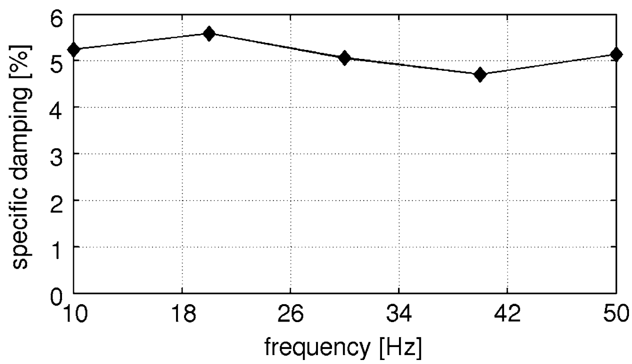

Fig. 20 Plot of specific damping as a function of frequency

6. The Role of Heat Effects in the Damping Capacity of SMAs

As reported above, the increasing frequency does not seem to affect the SDC which suggests that the superelastic damping is rate independent. However, such a conclusion is in clear contradiction with the results obtained on the same wire (Fig. 21) we recently published in Ref 9. In this paper, the superelastic damping capacity was investigated using the same experimental equipment except for the thermal chamber that was not used. The wire was simply exposed to the ambient temperature environment. In that case, a dramatic decrease of dissipated energy with increasing frequency was found. The fact that the thermal conditions of the wire surroundings influence the sensitivity of superelastic damping to the frequency (deformation rate) suggests that the thermal effects accompanying the MT (heat exchange with the environment) may be responsible for such a sensitivity. The mechanism how this happens, however, was not clear.

7. Modelling of the Heat Effects

In order to find out in which way the heat effects influence the superelastic damping of NiTi wire in tension, an earlier proposed phenomenological SMA model RLOOP (Ref 10) has been coupled with a lumped-capacity heat equation and used to simulate the fast superelastic deformation in Ref 11. The RLOOP model was originally developed (see Ref 10 for a detailed description) to simulate the key SMA responses to

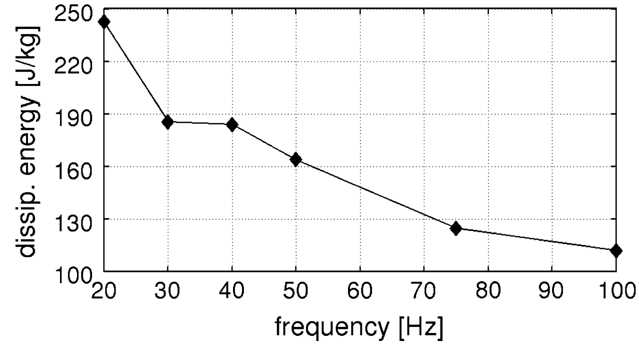

Fig. 21 Graph of dissipated energy vs. frequency published in Ref 9. The curve was measured on the same NiTi wire as the one analyzed in this paper. The measurement was performed at the room temperature without the use of the thermal chamber. The other measurement conditions were set up as follows: prestrain 4%, amplitude 1.2%, and frequency 50 Hz

general thermomechanical cyclic loads in tension, as e.g. actuator or recovery stresses generated in SMA composites. It assumes the existence of a general thermodynamic driving force for the MT when constructing a governing kinetics equation for the evolution of the martensite fraction ζ. The martensite phase fraction rate, $\dot{\zeta}$, is assumed to be a function of the driving force and its rate. The important features of the RLOOP algorithm are the rate independence of the simulated stress-strain-temperature responses and temperature independent hysteresis. The coupling of the RLOOP with the heat equation was done in such a way that the temperature T originally assumed as an independent parameter becomes an unknown variable coupled with the algorithm through the heat equation (see Ref 11 for details).

The applied lumped-capacity heat equation is based on the assumption of a homogeneous temperature field. Such an assumption is in contradiction to the commonly observed shear band propagation where the latent heat exchange occurs locally (Ref 12). Nevertheless, as shown in Ref 11, even such a simplified approach seems to capture the phenomena observed experimentally during superelastic cycling. Assuming a homogeneous temperature field, the wire temperature T in the RLOOP model becomes a variable governed by the heat equation. For a wire undergoing superelastic cycling at ambient environment with a constant temperature of the surrounding air $T_{\rm ext}$, the heat equation has to account for three most important heat sources—(i) the latent heat absorption/generation due to the stress induced MT, (ii) the heat generation due to the friction, and (iii) the convective heat exchange between the wire and its surrounding (see Fig. 22, Eq 1).

$$\begin{aligned} &c_v\dot{T} = q_{\rm lat} + q_{\rm conv} + q_{\rm fric} \\ &q_{\rm lat} = T\Delta s\dot{\zeta}{,}_{\rm conv} = -\frac{h}{\rho L}(TT_{\rm ext}), \\ &q_{\rm fric} = A\dot{\zeta} \end{aligned} \qquad \text{(Eq 1)}$$

The latent heat flow $q_{\rm lat}$ is defined as a product of the martensite fraction rate $\dot{\zeta}$, wire temperature T and the difference between the specific entropies of austenite and martensite Δs at a referential temperature. The heat flow $q_{\rm fric}$ expresses the heat assumed to be generated during the transformation process additionally to the latent heat. It is called "friction" and considered to take place during both the forward and reverse

MT. Due to lack of information about the friction heat flow, it is expressed as a linear function of the rate martensite fraction change. Although the heat exchange by convection q_{conv} represents a complex heat transfer mode, it is expressed in a commonly used way using the heat transfer coefficient h, the wire length L, and the temperature difference with respect to the temperature of surrounding T_{ext}. The wire is supposed to have a volume V, the specific mass ρ and the specific heat capacity c_v that is assumed to be the same for both phases. The model captures nearly all the apparently curious phenomena observed experimentally—i.e. (i) the variation and stabilization of the superelastic loop within the unsteady vibration range (Ref 11), (ii) the rate dependence of the hysteresis at strain rates for which the thermal conditions of cycling pass from isothermal to adiabatic (Ref 13).

The heat equation coupled RLOOP model was used to simulate the effect of the excitation frequency on the superelastic damping at ambient environment (Fig. 21). The heat convection considered in the heat equation allows only for limited heat transfer across the wire interface. The parameters of the heat equation that were used in the simulation of heat effects are listed in Table 2. The geometrical parameters of the wire were chosen according to the experimentally tested

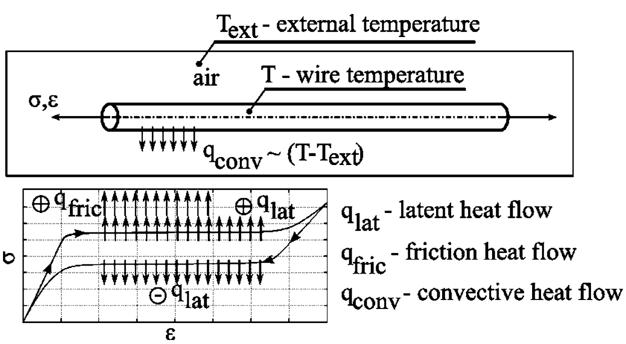

Fig. 22 All assumed heat processes taking place during the superelastic cycling

specimen, i.e. diameter 0.1 mm, gauge length 50 mm. The coefficient A in Eq 1 is computed according to Eq 2 based on the assumption that the hysteresis area of the stabilized superelastic loop at isothermal conditions ($h \rightarrow \infty$) represents the integral friction heat within one cycle (no energy dissipated to defects is assumed).

$$A = \frac{1}{\rho} \frac{\oint_{1\text{cycle at } T=T_{ext}} \sigma \dot{\varepsilon} dt}{\oint_{1\text{cycle at } T=T_{ext}} \dot{\zeta} dt} \qquad \text{(Eq 2)}$$

The simulation results are shown in Fig. 23. The model predicts that although the environmental temperature is constant, the temperature of the wire T evolves periodically during a single cycle (the left-hand side of Fig. 23) and the mean temperature increases toward stabilization with increasing number of cycles (the right-hand side of Fig. 23).

It should be noticed that the difference between the environment temperature and the stabilized value of the mean temperature of the wire dramatically increases with increasing frequency. The stabilization itself is due to the tendency of the system toward a heat balance over one cycle. It spreads into many cycles (~50-100) due to the limited constant rate of the heat exchange by convection requiring more cycles to reach the heat balance over one cycle (Ref 11). The simulated frequency dependence of the dissipated energy and SDC is shown in Fig. 24. Surprisingly, the model does not predict the experimentally observed decrease of the SDC with increasing frequency. One possible explanation is that the RLOOP simulation does not reflect the converging M_s A_f lines (Fig. 3) and thus cannot simulate the effect of temperature on the energy dissipation. However, when the simulation results are recalculated taking into account both the experimentally identified temperature dependency of the dissipated energy (Fig. 15) and the mean wire temperature evolution with respect to frequency, one obtains an exponentially decreasing dissipation energy with increasing frequency (Fig. 24) as it was observed experimentally in Ref 9 (Fig. 21). Apparently the decrease of the SDC with increasing frequency may be partially

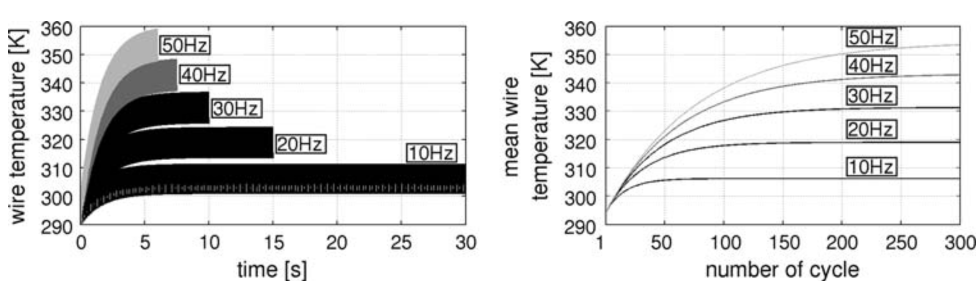

Fig. 23 Plot of the instantaneous wire temperature variation during cycling (left-hand side) and the mean wire temperature over one cycle vs. number of cycle (right-hand side)

Table 2 Parameters of RLOOP model and heat equation

M_s, K	E_a, GPa	σ_{re}, MPa	s, MPa/°C	G, 1/K	m	$k1$	c_v, J/kg/K	ρ, kg/m^3	T_{ext}, K	A_s, K	E_m, GPa	ε_{tr}, %	C, MPa/K	l	n	$k2$	Δs, J/kg/K	h, W/m^2/K
210	50	100	5.5	0.25	1	1	326	6450	293	250	21	5.2	50	1.1	5	1	54	35

M_s/A_s martensite/austenite start equation; E_a/E_m Young modulus of austenite/martensite; σ_{re} reorientation stress below M_f; s slope of the temperature dependence of the transformation start stresses; ε_{tr} transformation strain; G, c, l, m, n, $k1$, $k2$ fitting parameters; c_v specific heat capacity; Δs difference between specific entropies of austenite and martensite at referential temperature; h heat transfer coefficient; T_{ext} temperature of surroundings

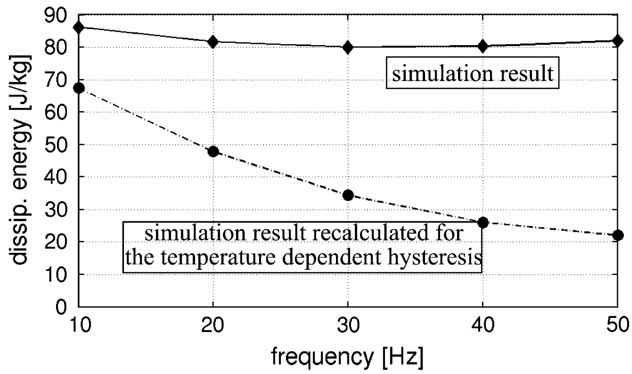

Fig. 24 Frequency evolution of dissipated energy predicted by simulation and recalculated using the experimentally identified temperature dependence of dissipated energy shown in Fig. 15

due to the combination of the temperature and frequency effects. For the discussion of the low frequency maximum see Ref 11, 13.

On the other hand, such a dramatic increase of the mean wire temperature with increasing frequency cannot be expected in case of the present experiment in which the temperature of the wire surroundings is actively controlled by the thermal chamber. The thermal chamber represents a heat sink absorbing the heat much more efficiently though the conditions are still very far from isothermal in the sense that the temperature variations within one cycle are still present.

The simulation and experimental results presented above thus lead us to a conclusion that the exponential decrease of the dissipated energy with frequency (Fig. 21) obtained without an active thermal control of surroundings is most likely due to the combined effect of the heat effects and material properties showing converging M_s and A_f lines (Fig. 3). In other words, as the stabilized mean wire temperature increases with frequency due to the heat effects, the dissipated energy in one cycle decreases due to the temperature dependence of the superelastic hysteresis being a specific property of the studied wire. Such a property was experimentally evidenced in the quasistatic regime by the constructed stress-temperature diagram (Fig. 3) and in the dynamic regime by the identified temperature dependence of the dissipated energy (Fig. 15). If the temperature of the wire is actively controlled by the environmental chamber, the dramatic increase of the mean temperature of the wire in the stabilized regime does not occur and the effect of increasing frequency on the dissipated energy and SDC is negligible. Nevertheless, since the SMA dampers are not commonly put in thermal chambers and wires thicker than 0.1 mm are commonly used, it is essential to realize the heat transfer across the wire is in fact a very important fifth condition affecting the superelastic damping of SMA elements.

8. Conclusions

The superelastic damping of NiTi wires was investigated with regard to their use in passive damping applications. Four parameters—vibration amplitude, prestrain, temperature of surroundings and frequency—were identified as having the most pronounced influence on the superelastic damping. The influence of those parameters on the superelastic damping of a commercially available superelastic NiTi wire was experimentally investigated using a self-developed dynamical tester. The experimental investigation was carried out assuming that the influence of each of the four considered parameters is independent of the variation of the others. Since this is not true generally, a limited set of parameters around basal conditions corresponding to the prestrains within the plateau range, strain amplitudes $<2\%$, T = 20-65 °C, and frequencies 10-50 Hz.

The superelastic damping capacity of a commercial NiTi wire (d-0.1 mm)

- decreases by as much as 60% with increasing prestrain within the plateau range
- increases dramatically with increasing strain amplitude, a minimum vibration amplitude of 0.5% is required to initialize the superelastic damping
- decreases by as much as 60% with increasing temperature in the interval 10-65 °C. This was attributed to the temperature dependent stress hysteresis.
- remains approximately constant with increasing frequency in the interval 10-50 Hz in case the wire is in the thermal chamber controlling actively the environmental temperature. In case of free wire (no thermal chamber) used in actual damping applications, the superelastic damping capacity, however, significantly decreases with increasing frequency. This was explained as a combined effect of the heat effects affecting the mean wire temperature and material properties with the help of simulations using the heat equation coupled phenomenological SMA model.

References

1. Y. Liu, Z. Zeliang Xie, and J. Humbeeck, Cyclic Deformation of NiTi Shape Memory Alloys, *Mater. Sci. Eng. A*, 1999, **273–275**, p 673–678
2. D. Wolons, F. Gandhi, and B. Malovrh, Experimental Investigation of the Pseudoelastic Hysteresis Damping Characteristics of Shape Memory Alloy Wires, *J. Intell. Mater. Syst. Struct.*, 1998, **9**, p 116–126
3. F. Gandhi and G. Chapuis, Passive Damping Augmentation of a Vibrating Beam Using Pseudoelastic Shape Memory Alloy, *J. Sound Vib.*, 2002, **250**(3), p 519–539
4. F. Mazzolai, A. Biscarini, B. Coluzzi, G. Mazzolai, E. Villa, and A. Tuissi, Low-Frequency Internal Friction of Hydrogen-Free and Hydrogen-Doped NiTi Alloys, *Acta Mater.*, 2007, **55**, p 4243–4252
5. S.K. Wua and H.C. Linb, Damping Characteristics of TiNi Binary and Ternary Shape Memory Alloys, *J. Alloys Compd.*, 2003, **355**, p 72–78
6. S. Nemat-Nasser and W. Guo, Superelastic and Cyclic Response of NiTi SMA at Various Strain Rates and Temperatures, *Mech. Mater.*, 2006, **38**, p 463–474
7. M.C. Piedboeuf and R. Gauvin, Damping Behaviour of Shape Memory Alloys: Strain Amplitude, Frequency and Temperature Effects, *J. Sound Vib.*, 1998, **215**(5), p 885–901
8. http://www.avalon-eu.org
9. L. Heller, et al., Quasistatic and Dynamic Functional Properties of Thin Superelastic Wires, *Eur. Phys. J. Spec. Top.*, 2008, **128**, p 7–15
10. P. Sittner, R. Stalmans, and M. Tokuda, An Algorithm for Prediction of the Hysteretic Responses of Shape Memory Alloys, *Smart Mater. Struct.*, 2000, **9**, p 452–465
11. L. Heller, P. Sittner, and J. Pilch, Impact of Heat Effects on Superelasticity, *Proceedings of ICOMAT 2008*, 29/6 to 5/7/2008, Santa Fe, New Mexico, submitted
12. P. Sittner, Y. Liu, and V. Novak, On the Origin of Luders-Like Deformation of NiTi Shape Memory Alloys, *J. Mech. Phys. Solids*, 2005, **53**, p 1719–1746
13. J. Van Humbeeck and L. Delaey, The Influence of Strain-Rate, Amplitude and Temperature on the Hysteresis of a Pseudoelastic Cu-Zn-Al Single Crystal, *J. Phys.*, 1981, Col C5, Tome 42, p C5-1007-1011